LETTERS
PUBLISHED ONLINE: 2 OCTOBER 2017 | DOI: 10.1038/NMAT4994
nature materials

Organoid cystogenesis reveals a critical role of microenvironment in human polycystic kidney disease

Nelly M. Cruz[1,2,3,4], Xuewen Song[5,6], Stefan M. Czerniecki[1,2,3,4], Ramila E. Gulieva[1,2,3,4], Angela J. Churchill[1,2,3,4], Yong Kyun Kim[1,2,3,4], Kosuke Winston[1,2,3,4], Linh M. Tran[1,2,3,4], Marco A. Diaz[1,2,3,4], Hongxia Fu[3,4,7,8], Laura S. Finn[9,10], York Pei[5,6], Jonathan Himmelfarb[1,2,4] and Benjamin S. Freedman[1,2,3,4]*

Polycystic kidney disease (PKD) is a life-threatening disorder, commonly caused by defects in polycystin-1 (PC1) or polycystin-2 (PC2), in which tubular epithelia form fluid-filled cysts[1,2]. A major barrier to understanding PKD is the absence of human cellular models that accurately and efficiently recapitulate cystogenesis[3,4]. Previously, we have generated a genetic model of PKD using human pluripotent stem cells and derived kidney organoids[5,6]. Here we show that systematic substitution of physical components can dramatically increase or decrease cyst formation, unveiling a critical role for microenvironment in PKD. Removal of adherent cues increases cystogenesis 10-fold, producing cysts phenotypically resembling PKD that expand massively to 1-centimetre diameters. Removal of stroma enables outgrowth of PKD cell lines, which exhibit defects in PC1 expression and collagen compaction. Cyclic adenosine monophosphate (cAMP), when added, induces cysts in both PKD organoids and controls. These biomaterials establish a highly efficient model of PKD cystogenesis that directly implicates the microenvironment at the earliest stages of the disease.

PKD affects one in ∼1,000 people worldwide, with no known cure[1,2]. Animal models do not fully genocopy or phenocopy human PKD, and are too complex physiologically for a minimal reconstitution approach[7–10]. A human cellular model is needed to complement animal models and reveal the early pathophysiology of PKD. We have generated human pluripotent stem cells (hPSCs) with targeted, biallelic mutations that lack the mature form of PC1, or any detectable PC2, using the Cas9/CRISPR (clustered regularly interspaced short palindromic repeats) gene editing system (Supplementary Fig. 1a,b)[6,11]. Under adherent culture conditions, kidney organoids derived from *PKD1*$^{-/-}$ or *PKD2*$^{-/-}$ hPSCs form fluid-filled cysts, although cystogenesis is highly inefficient (∼7% of organoids), and its mechanism has not been determined[6]. We used this system as a starting point to investigate how cysts form and identify modulators of cystogenesis. Time-lapse imaging revealed that cyst formation involved two steps: first, rearrangement of a tubule within an organoid, resulting in deformation of linear shape to form a 'pre-cyst' surrounding an hollow pocket; and second, partial detachment of the pre-cyst from the underlying stratum followed immediately by rapid expansion, resulting in a buoyant cyst tethered to an adherent organoid remnant (Fig. 1a and Supplementary Fig. 1c,d, and Supplementary Movie 1). Cysts therefore arose from whole tubular segments that expanded and partially detached from the adherent surface.

On the basis of these results, we hypothesized that adherent forces played a critical role in limiting tubular deformation and subsequent cyst formation. To test this, organoids were purified on day 21 of differentiation, prior to the formation of cysts, and transferred to wells coated with an anti-adhesive hydrogel to generate suspension cultures (Fig. 1b and Supplementary Fig. 1e, and Supplementary Movie 2). After two weeks in suspension, ∼75% of PKD organoids formed large, free-floating cysts (Fig. 1c,d), a 10-fold increase in cyst formation over adherent cultures[6]. Control organoids of identical genetic background formed cysts only very rarely under these conditions, indicating that cystogenesis remained a specific consequence of the PKD mutations (Fig. 1c,d). As an inherent property of this differentiation system in both PKD and control cultures, each of the organoids placed into suspension was relatively small (∼250 μm in diameter) and contained only ∼5 tubules, therefore a significant proportion (∼15%) of individual tubules deformed into cysts. In long-term cultures, PKD cysts further expanded massively and reached diameters of ∼1 centimetre, reflecting a 4,000-fold increase in size over the original organoid (Fig. 1e). Even after many months in suspension, cysts remained rare among control organoids, which formed smaller, denser aggregates (Fig. 1d,e). Thus, modification of the material environment enabled the establishment of a highly efficient minimal reconstitution system for PKD cystogenesis.

[1]Division of Nephrology, University of Washington School of Medicine, Seattle, Washington 98109, USA. [2]Kidney Research Institute, University of Washington School of Medicine, Seattle, Washington 98109, USA. [3]Institute for Stem Cell and Regenerative Medicine, University of Washington School of Medicine, Seattle, Washington 98109, USA. [4]Department of Medicine, University of Washington School of Medicine, Seattle, Washington 98109, USA. [5]Division of Nephrology, University Health Network, Toronto, Ontario M5G2N2, Canada. [6]University of Toronto, Toronto, Ontario M5G2N2, Canada. [7]Division of Hematology, Department of Medicine, University of Washington School of Medicine, Seattle, Washington 98109, USA. [8]Department of Bioengineering, University of Washington School of Medicine, Seattle, Washington 98109, USA. [9]Department of Pathology, University of Washington School of Medicine, Seattle, Washington 98105, USA. [10]Department of Laboratories, Seattle Children's Hospital, Seattle, Washington 98105, USA. *e-mail: benof@uw.edu

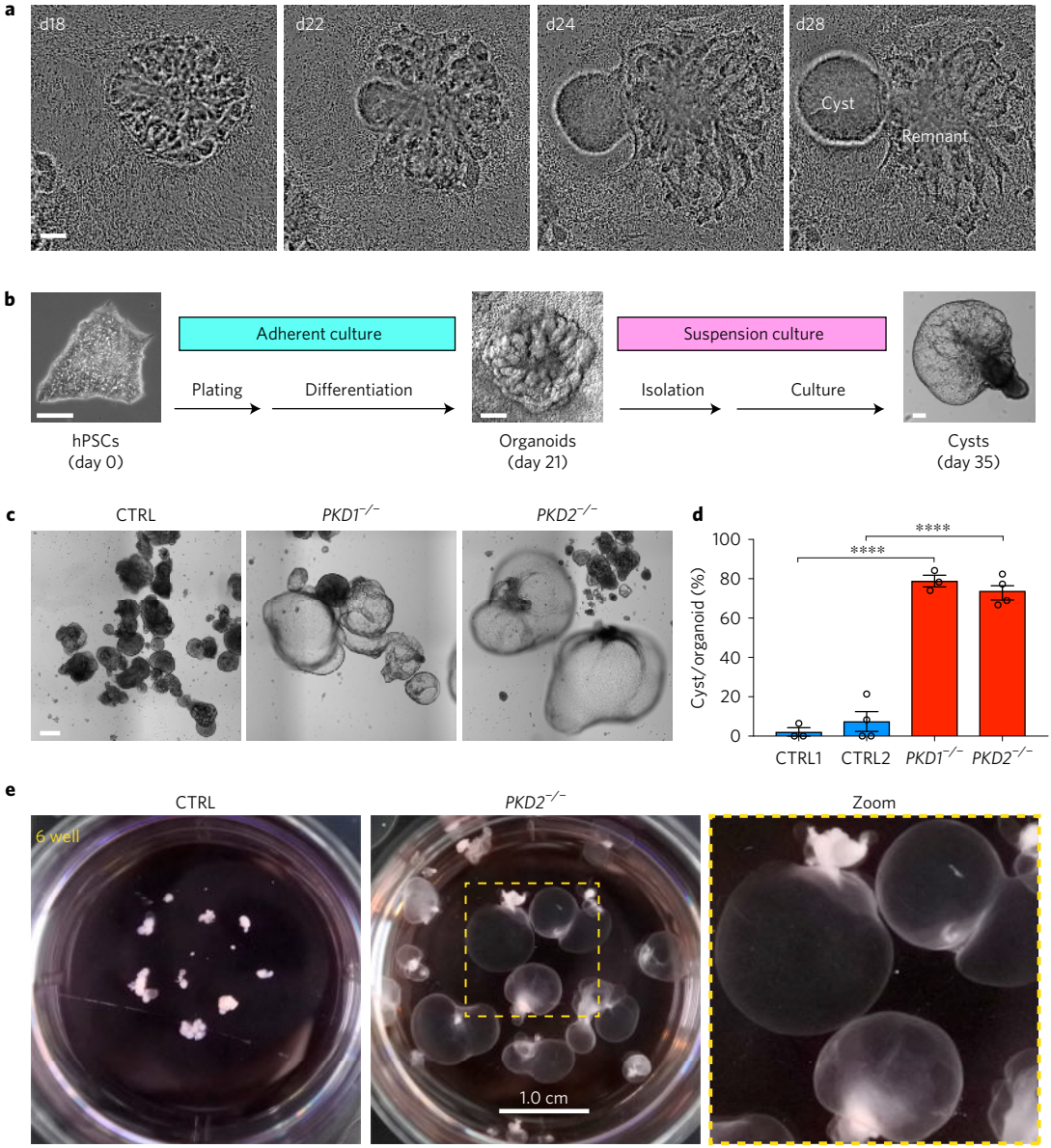

Figure 1 | Removal of adherent cues establishes a highly efficient model of PKD cystogenesis. a, Still images from Supplementary Movie 1 showing cyst formation from a PKD organoid in adherent culture. **b**, Schematic of high-efficiency organoid cystogenesis protocol. **c**,**d**, Representative images of kidney organoids (**c**) and quantification of cyst formation after two weeks of suspension culture (**d**) (CTRL1 versus *PKD1*$^{-/-}$, $n=3$ separate experiments, ±s.e.m., $t(3.663)=21.05$, $p=5.8949\times10^{-5}$; CTRL2 versus *PKD2*$^{-/-}$, $n=4$ separate experiments, ±s.e.m., $t(5.458)=10.66$, $p=7.3731\times10^{-5}$). **e**, 6-well (3.5 cm) dishes containing PKD or control organoids after nine months of culture. Zoom is shown of dashed box region. Scale bars, 100 μm (**a**–**c**) and 1 cm (**e**).

Histological analysis revealed that PKD organoid cysts were lined with a thin, squamous epithelial layer, approximately one single cell in thickness, with irregular edges, surrounding a hollow lumen (Fig. 2a). When compared to cysts from various stages and subtypes of clinical PKD *in vivo*, organoid cysts most closely resembled cysts in prenatal PKD, which extended radially from the medulla to the cortex and appeared prominent just beneath the nephrogenic zone (Fig. 2a and Supplementary Fig. 2a). Similar cysts were previously reported in patients with biallelic mutations in *PKD1* (ref. 12). In contrast, postnatal cysts from patients exhibited a more smooth-edged and multi-layered appearance, and were accompanied by interstitial nephritis and inflammatory infiltrates not observed prenatally or in organoids (Fig. 2a and Supplementary Fig. 2a).

We previously identified *Lotus tetragonolobus* lectin (LTL) and E-cadherin (ECAD), respectively, as markers of organoid proximal and distal tubules in these cultures[6]. In non-cystic organoids and tissues, these markers were not mutually exclusive, but rather formed a continuum, with enrichment in their respective nephron segments (Supplementary Fig. 2b). In PKD organoid cysts, LTL and ECAD largely overlapped within the cyst-lining epithelium, exhibiting patches of specific enrichment, whereas PODXL, a marker enriched in kidney podocytes, was not detected in cysts, similar to prenatal and postnatal PKD patient kidneys (Fig. 2b,c and Supplementary Fig. 2c)[12–14]. Approximately 80% of organoid cysts expressed both LTL and ECAD, which were also detected within the tubular remnants continuous with these cysts (Fig. 2b–f and Supplementary Fig. 2c). Cyst-lining cells in organoids were heavily coated with primary cilia and formed tight junctions between cells in a cobblestone pattern (Fig. 2g). Interestingly, organoid cysts in long-term suspension cultures also contained a subpopulation of stromal cells that co-expressed smooth muscle α-actin (SMA) and

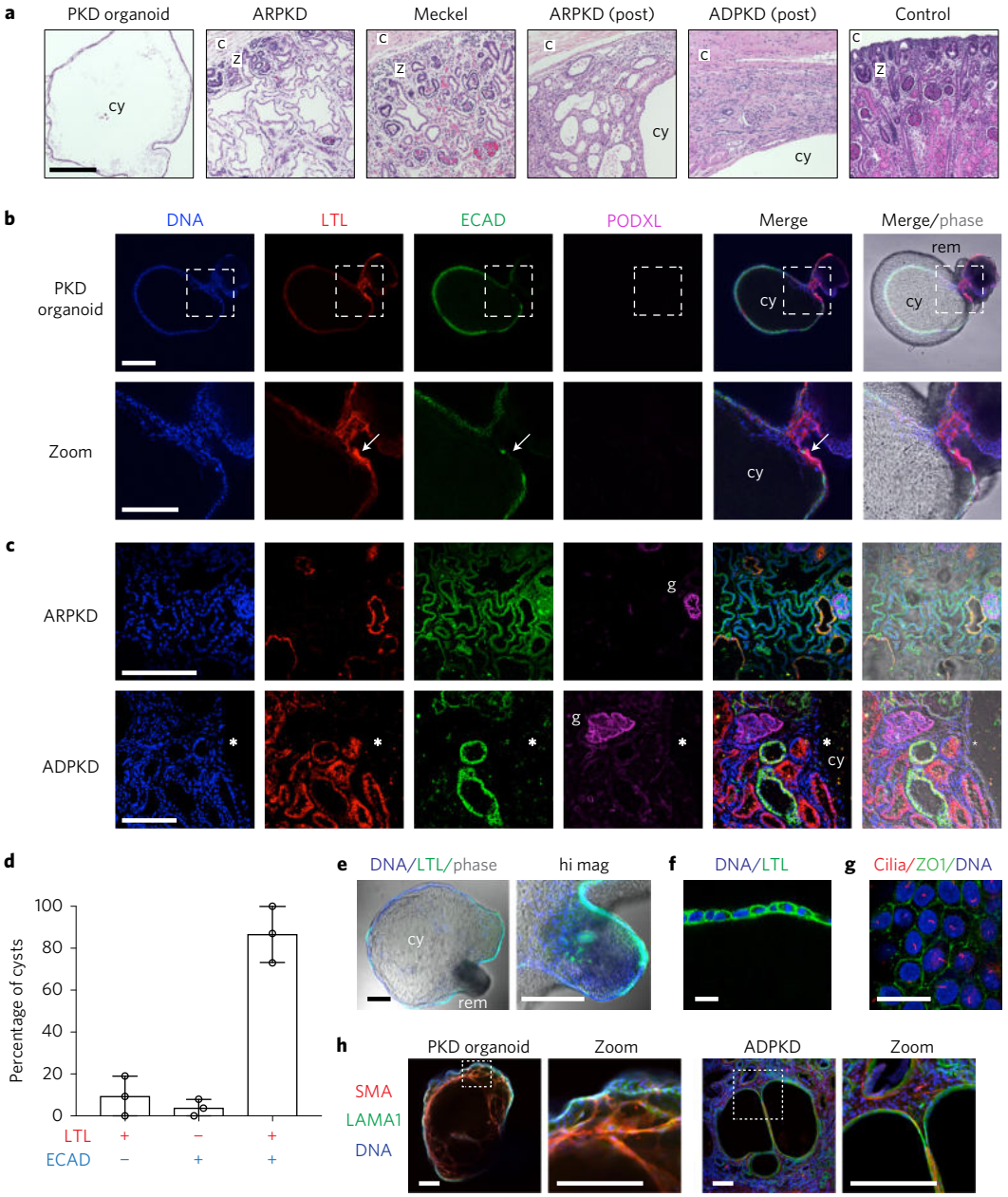

Figure 2 | Organoid PKD cysts phenotypically resemble PKD patient cysts. a, Paraffin sections dyed with haematoxylin and eosin from PKD organoids, or human kidney biopsies taken from patients with autosomal dominant PKD (ADPKD), autosomal recessive PKD (ARPKD), and Meckel syndrome. Identifying labels are provided for orientation and emphasis of specific histological features (c, kidney capsule; z, nephrogenic zone; cy, large cyst; post, postnatal). **b**,**c**, Confocal immunofluorescence showing nephron segment markers in PKD organoid cysts (**b**) or PKD patient kidneys (**c**). Zoom shows close-up of dotted boxed region. Arrow represents an area of specific enrichment for LTL. Glomeruli (g) do not appear cystic. Neither LTL nor ECAD is detected in a large ADPKD cyst, whose epithelium has dedifferentiated (*). **d**, Percentage of PKD organoid cysts labelling positive for LTL, ECAD, or both markers ($n = 3$ separate experiments, ±s.e.m.). **e**, Confocal optical sections showing LTL affinity in a representative cyst in suspension. Higher-magnification (hi mag) image shows LTL in the adjoining organoid remnant portion of this cyst. **f**, LTL in cyst-lining epithelial cells. **g**, Cilia (acetylated α-tubulin) and tight junctions (ZO1) in representative cyst-lining epithelial cells. **h**, Representative confocal images showing stromal markers in PKD organoid cyst and patient cysts. Scale bars, 200 μm or 25 μm (**f**,**g**).

laminin, markers expressed in cystic stroma of PKD patient kidneys (Fig. 2h and Supplementary Fig. 2d). Collagen deposition in these cysts remained scant, similar to cysts in prenatal PKD kidneys, whereas postnatal PKD kidney cysts exhibited prominent fibrosis (Supplementary Fig. 2e). PKD organoid cysts *in vitro* therefore recapitulated hallmark features of PKD patient cysts, particularly the very early stages of PKD.

PKD organoid cysts in adherent cultures exhibited a two-fold increase in phosphorylated histone H3 (pH3), compared to LTL^+ tubular cells from non-mutants, indicating increased proliferation (Fig. 3a,b). Similarly, in large cysts in long-term suspension cultures, dividing cells were detected within the cyst-lining epithelium and in anaphases oblique and internal to the plane of the cyst (Fig. 3c and Supplementary Fig. 3a,b and Supplementary Movie 3). When large PKD cysts were microdissected away from their remnant tubules, they immediately deflated, reflecting the loss of accumulated fluid (Fig. 3d). Cysts contained from ~30,000 to ~600,000 cells, whereas the original organoids from which

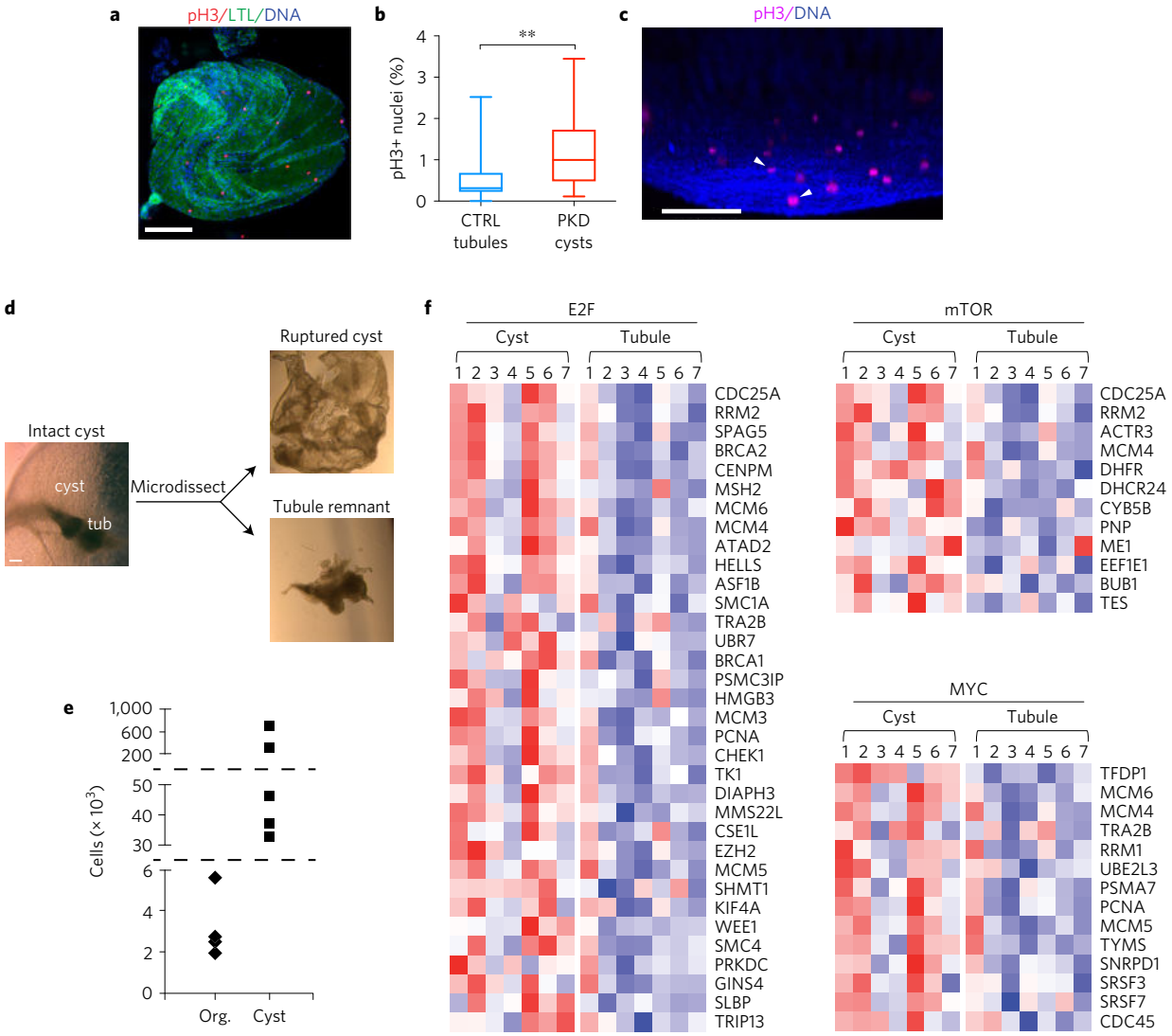

Figure 3 | PKD organoid cysts arise from hyperproliferative KTECs. a,**b**, Representative images (**a**) and quantification of pH3 (**b**) in adherent PKD organoid cysts under adherent conditions. Boxes show 25th and 75th percentiles, whiskers indicate min and max values ($n = 115$ tubules pooled from seven separate experiments and 26 cysts pooled from six separate experiments, ±s.e.m., $t(37.16) = 3.491$, $p = 0.0013$). **c**, Three-dimensional confocal reconstruction of a large cyst in suspension. Arrowhead indicates anaphases. See also Supplementary Movie 3. **d**, Representative images showing microdissection of large cysts in suspension. **e**, Cell counts in organoids immediately after placement in suspension (Org.) or in microdissected cysts grown for several months (Cyst). Dashed lines represent nonlinear breaks in the *y*-axis. **f**, Heat maps from microarray analysis of cysts and tubule remnants from cultured organoids, showing differentially expressed genes (p-value ≤ 0.05) contributing to activation of E2F targets, mTORC1 signalling, and MYC. Columns represent samples and row represents gene; red indicates greater than the mean (white) and blue, less than the mean values. Scale bars, 100 μm.

they derived contained only ~3,000 cells, indicating extensive proliferation (Fig. 3e). Pathway-based global gene expression microarray analysis revealed significant enrichment of hallmark gene sets for cell cycle progression, mTOR signalling, and MYC activity in cysts, compared to remnant tubules (Fig. 3f). PKD cysts therefore arose from hyperproliferative kidney tubular epithelial cells (KTECs), a hallmark of mouse and human autosomal dominant PKD (ADPKD)[8,9,14,15].

The process of purifying organoids and transferring them into suspension might induce cyst formation by provoking an injury response[16,17]. To test this, organoids were purified and immediately replated onto wells coated with a thin layer of extracellular matrix (ECM) but lacking stroma. The replated organoids re-adhered but did not form cysts, indicating that injury alone was not sufficient to promote cystogenesis (Fig. 4a). Under these conditions, we observed that both control and PKD organoids formed expanding cell outgrowths very quickly, which could be further expanded as monolayers up to three passages (Fig. 4a and Supplementary Fig. 3c). Cells derived from organoid outgrowths exhibited a cobblestone-like epithelial morphology and predominantly expressed markers specific to KTECs, including LTL and kidney injury molecule-1 (KIM-1), similar to flow-sorted LTL^+ cells from organoid cultures (Fig. 4b–d and Supplementary Fig. 3d,e). Removal of stroma thus stimulated proliferation and migration of organoid cells.

We further utilized these organoid KTEC cell lines to investigate the expression of PC1, whose structure suggests a possible role in cell adhesion[18,19]. In contrast to many cell types, KTECs derived from organoid outgrowths expressed sufficient quantities of endogenous PC1 to detect in lysates by immunoblot (Fig. 4e)[20,21]. Surprisingly, we found that PC1 protein was nearly undetectable in KTECs derived from $PKD2^{-/-}$ organoids, using an antibody against the amino terminal fragment (Fig. 4e)[22]. Undifferentiated $PKD2^{-/-}$ hPSCs exhibited a similarly strong decrease

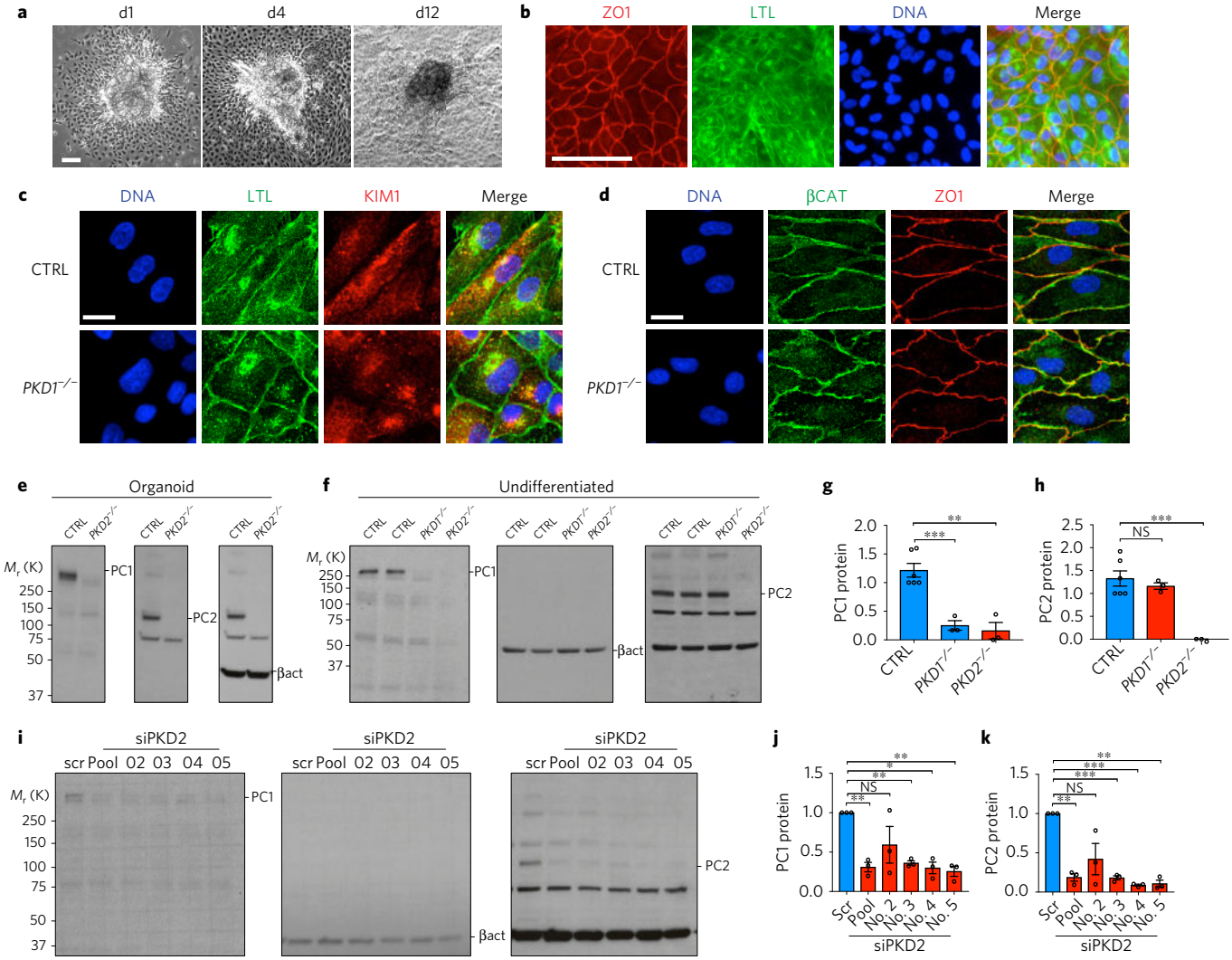

Figure 4 | Outgrowth of PKD cell lines reveals a critical deficiency in PC1 expression. a, Phase-contrast image of organoid explants on days 1, 4, and 12 after replating. **b**–**d**, Wide-field fluorescence (**b**) and confocal sections (**c**,**d**) showing epithelial and kidney-specific marker expression in representative kidney organoid cell monolayers. **e**,**f**, Representative immunoblots of PC1 and PC2 in kidney organoids (**e**) and undifferentiated hPSCs (**f**). **g**, PC1 protein levels in undifferentiated hPSCs, normalized to β-actin loading control (CTRL, $n=6$; $PKD1^{-/-}$ and $PKD2^{-/-}$, $n=3$, ±s.e.m., CTRL versus $PKD1^{-/-}$, $t(6.936)=6.603$, $p=0.00031$ (***); CTRL versus $PKD2^{-/-}$, $t(4.837)=5.669$, $p=0.0026$ (**)). **h**, PC2 protein levels in undifferentiated hPSCs, normalized to β-actin loading control (CTRL, $n=6$; $PKD1^{-/-}$ and $PKD2^{-/-}$, $n=3$, ± s.e.m., CTRL versus $PKD1^{-/-}$, $t(6.451)=0.9247$, $p=0.3884$ (NS); CTRL versus $PKD2^{-/-}$, $t(5)=8.006$, $p=0.0005$ (***)). **i**–**k**, Representative immunoblot (**i**) and quantification of PC1 and PC2 levels (**j**,**k**) in hPSCs treated with four different *PKD2* siRNAs (pooled or individually) or a scrambled (Scr) siRNA control ($n=3$). Statistical analysis: **j**, Unpaired *t*-test with Welch's correction, Scr versus pool, $t(2)=11$, $p=0.0075$; No. 2 versus Scr, $t(2)=1.747$, $p=0.2227$; No. 3 versus Scr, $t(2)=22.66$, $p=0.0019$; No. 4 versus Scr, $t(2)=9.467$, $p=0.0110$; No. 5 versus Scr, $t(2)=11.56$, $p=0.0074$. **k**, Unpaired *t*-test with Welch's correction, Scr versus pool, $t(2)=16.92$, $p=0.0035$; No. 2 versus Scr, $t(2)=2.912$, $p=0.1005$ (NS, not significant); No. 3 versus Scr, $t(2)=31.93$, $p=0.0010$; No. 4 versus Scr, $t(2)=77.64$, $p=0.0002$; No. 5 versus Scr, $t(2)=20.28$, $p=0.0024$. Scale bars, 100 μm (**a**,**b**) or 10 μm (**c**,**d**). NS, not significant.

in PC1 expression levels (Fig. 4f,g). *PKD1* transcripts were expressed at normal levels in $PKD2^{-/-}$hPSCs, suggesting that PC1 loss occurs through a post-transcriptional mechanism (Supplementary Fig. 4a,b). Conversely, in $PKD1^{-/-}$ cells, PC2 expression levels were unchanged from isogenic controls, although its localization to primary cilia was strikingly decreased, consistent with previous reports (Fig. 4f,h and Supplementary Fig. 4c–e)[5,20,21]. Furthermore, treatment of control hPSCs with three different siRNAs, which knocked down PC2 protein to 12.6 ± 0.02% of normal levels (avg. ± s.e.m.), induced a corresponding decrease in PC1 protein to 30.5 ± 0.03% of normal levels (Fig. 4i–k). These studies revealed, unexpectedly, that PC2 was required for PC1 amino-terminus expression in human cells, in contrast to reports in mouse $Pkd2^{-/-}$ cells[20,21]. Differences between species, cell types, or exogenous versus endogenous expression levels may account for this discrepancy, as PC1 is a low-abundance protein in humans, who appear to be highly sensitive to reductions in its expression, compared to mice[6,7,23,24].

A unifying hypothesis that emerges from these studies is that the ECM microenvironment functions to maintain tubular shape and adhesion through interactions involving PC1's long, extracellular domain[18,19,25]. To directly test the effect of PKD mutations on the matrix microenvironment, we embedded individual organoids (~250 μm diameter) into larger collagen droplets (~4 mm diameter), and placed these in suspension. Droplets implanted with organoids did not form cysts, but rather contracted dramatically over a period of approximately 1–2 weeks (Fig. 5a). $PKD1^{-/-}$ organoids were quantitatively impaired in their ability to compact

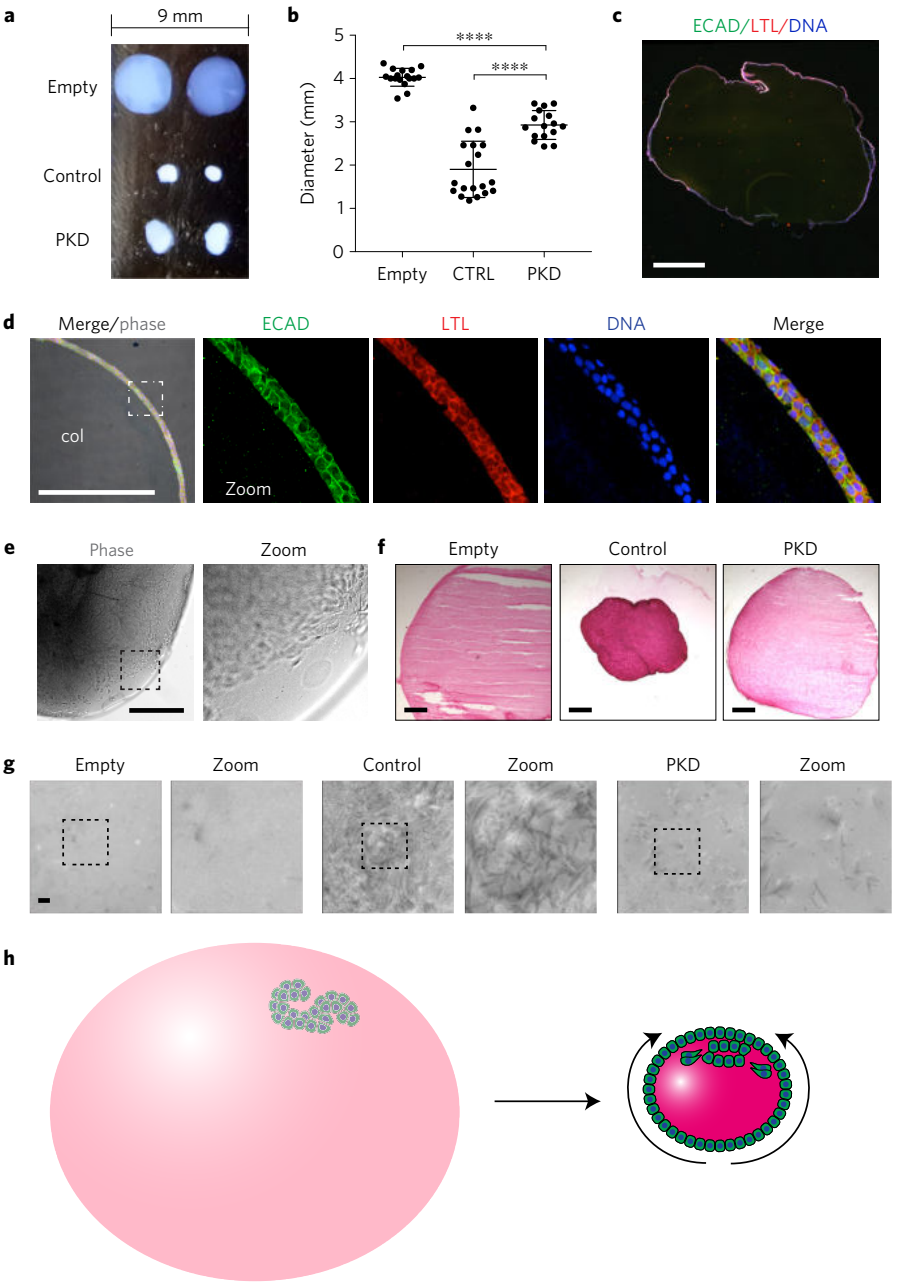

Figure 5 | Organoids remodel their matrix microenvironment in a PKD-dependent manner. a, Photograph of organoids implanted into collagen balls and cultured in suspension for two weeks. **b**, Diameters of empty ($n=17$) and organoid-implanted (CTRL, $n=19$; PKD, $n=16$) collagen droplets, pooled from three experiments (empty versus CTRL, $t(21.96)=13.53$, $p=3.9334\times10^{-12}$; CTRL versus PKD, $t(24.74)=11.33$, $p=1.7989\times10^{-6}$). Each droplet is indicated by a single data point. **c**, Wide-field immunofluorescence image of whole droplet compacted by a PKD organoid, stained for tubule segment markers. **d**, Confocal immunofluorescence at the edge of a representative droplet after contraction, adjacent to the collagen interior (col). The dashed boxed region is shown for each individual channel at higher magnification. **e**, Phase-contrast images showing the edge of a representative droplet at an early stage of compaction, with zoom of dashed boxed region. **f**, Sirius red staining of collagen droplets. **g**, TEM 25,000× images of collagen filament structure in the interior of droplets. Zoom of dashed boxed region is shown for each image. **h**, Schematic of collagen droplet compaction by organoids. KTECs migrate out and surround the scaffold, which contracts towards the outgrowth (curved arrows). Scale bars, 500 μm (**c**–**f**) or 500 nm (**g**).

collagen droplets, compared to isogenic controls (Fig. 5b). Contracted droplets comprised an inner core of solid collagen encompassed by a thin, continuous epithelium of $LTL^{+}ECAD^{+}$ KTECs (Fig. 5c,d). During the formation of these structures, KTECs could be observed migrating out of the implanted organoid to coat the surface of the droplet (Fig. 5e). Collagen staining appeared more intense after contraction, and collagen fibres appeared denser ultrastructurally, indicating that the changes in droplet size involved physical compression (Fig. 5f,g). Collectively, these findings revealed that kidney organoid epithelia were capable of dramatically remodelling their ECM microenvironment through migratory forces, and that this property was partially dependent on PC1 (Fig. 5h).

cAMP signalling is hypothesized to contribute significantly to PKD, but can also promote fluid accumulation in non-PKD epithelia[3,26]. Forskolin, a powerful agonist of adenylyl cyclase,

induced rapid and dose-dependent swelling of adherent organoids into round, cyst-like structures that retained the shape of the original tubules (Supplementary Fig. 5a,b and Supplementary Movie 4). The non-degradable cAMP analog 8-Br-cAMP also induced swelling, although the effect was much less pronounced (Supplementary Fig. 5b,c). Upon withdrawal of these agents, the swollen structures deflated and the organoids returned towards their original size (Supplementary Fig. 5a–c). Both PKD and non-PKD organoids swelled and deflated to a similar degree after cAMP stimulation, indicating a modifier effect (Supplementary Fig. 5a–d and Supplementary Movie 4). One limitation of this system is that we were unable to examine collecting ducts, which are the primary target of cAMP-mediated candidate therapeutics[10,27], because these structures do not mature in kidney organoids[6,28–30].

In addition to gene-edited mutants, we also investigated the potential of using induced pluripotent stem cells (iPSCs) derived from PKD patients to model disease[5]. We found that iPSCs from human patients exhibited dramatic line-to-line variability in their abilities to form organoids, regardless of PKD genotype and organoid differentiation protocol (Supplementary Fig. 6a–c). The morphology of tubular structures also varied noticeably between different lines (Supplementary Fig. 6c). As such differences reflected a degree of heterogeneity that would confound analysis of PKD-specific effects, we focused our studies on the CRISPR-mutant hPSCs. Although patient-derived organoids presented much variability, they could eventually represent valuable tools to develop personalized medicine approaches.

In conclusion, by combining PKD organoids with modular physical environments, we have established a human cellular system that models PKD with high efficiency and specificity. Comparison of PKD and non-PKD organoids suggests a specific, primary role for microenvironment and adhesion in early stages of the disease. Interventions that strengthen stromal or scaffolding components can provide a critical cue favouring migratory repair over cystogenesis. Our biochemical studies indicate a central requirement for PC1, which we propose functions as an adhesion regulator that maintains tubular architecture through interactions with the microenvironment. The efficiency, specificity, and modularity of organoid cultures provide critical insight into the biomaterial basis of human disease, with great potential for mechanistic studies and therapeutics development.

Methods

Methods, including statements of data availability and any associated accession codes and references, are available in the online version of this paper.

Received 18 January 2017; accepted 29 August 2017; published online 2 October 2017

References

1. The European Polycystic Kidney Disease Consortium. The polycystic kidney disease 1 gene encodes a 14 kb transcript and lies within a duplicated region on chromosome 16. *Cell* **77,** 881–894 (1994).
2. Mochizuki, T. *et al*. PKD2, a gene for polycystic kidney disease that encodes an integral membrane protein. *Science* **272,** 1339–1342 (1996).
3. Neufeld, T. K. *et al*. *In vitro* formation and expansion of cysts derived from human renal cortex epithelial cells. *Kidney Int.* **41,** 1222–1236 (1992).
4. Boletta, A. *et al*. Polycystin-1, the gene product of PKD1, induces resistance to apoptosis and spontaneous tubulogenesis in MDCK cells. *Mol. Cell* **6,** 1267–1273 (2000).
5. Freedman, B. S. *et al*. Reduced ciliary polycystin-2 in induced pluripotent stem cells from polycystic kidney disease patients with PKD1 mutations. *J. Am. Soc. Nephrol.* **24,** 1571–1586 (2013).
6. Freedman, B. S. *et al*. Modelling kidney disease with CRISPR-mutant kidney organoids derived from human pluripotent epiblast spheroids. *Nat. Commun.* **6,** 8715 (2015).
7. Lantinga-van Leeuwen, I. S. *et al*. Lowering of Pkd1 expression is sufficient to cause polycystic kidney disease. *Hum. Mol. Genet.* **13,** 3069–3077 (2004).
8. Shillingford, J. M. *et al*. The mTOR pathway is regulated by polycystin-1, and its inhibition reverses renal cystogenesis in polycystic kidney disease. *Proc. Natl Acad. Sci. USA* **103,** 5466–5471 (2006).
9. Trudel, M. *et al*. C-myc-induced apoptosis in polycystic kidney disease is Bcl-2 and p53 independent. *J. Exp. Med.* **186,** 1873–1884 (1997).
10. Gattone, V. H. II, Wang, X., Harris, P. C. & Torres, V. E. Inhibition of renal cystic disease development and progression by a vasopressin V2 receptor antagonist. *Nat. Med.* **9,** 1323–1326 (2003).
11. Jinek, M. *et al*. A programmable dual-RNA-guided DNA endonuclease in adaptive bacterial immunity. *Science* **337,** 816–821 (2012).
12. Vujic, M. *et al*. Incompletely penetrant PKD1 alleles mimic the renal manifestations of ARPKD. *J. Am. Soc. Nephrol.* **21,** 1097–1102 (2010).
13. Nakanishi, K., Sweeney, W. E. Jr, Zerres, K., Guay-Woodford, L. M. & Avner, E. D. Proximal tubular cysts in fetal human autosomal recessive polycystic kidney disease. *J. Am. Soc. Nephrol.* **11,** 760–763 (2000).
14. Grantham, J. J., Geiser, J. L. & Evan, A. P. Cyst formation and growth in autosomal dominant polycystic kidney disease. *Kidney Int.* **31,** 1145–1152 (1987).
15. Song, X. *et al*. Systems biology of autosomal dominant polycystic kidney disease (ADPKD): computational identification of gene expression pathways and integrated regulatory networks. *Hum. Mol. Genet.* **18,** 2328–2343 (2009).
16. Takakura, A. *et al*. Renal injury is a third hit promoting rapid development of adult polycystic kidney disease. *Hum. Mol. Genet.* **18,** 2523–2531 (2009).
17. Patel, V. *et al*. Acute kidney injury and aberrant planar cell polarity induce cyst formation in mice lacking renal cilia. *Hum. Mol. Genet.* **17,** 1578–1590 (2008).
18. The International Polycystic Kidney Disease Consortium. Polycystic kidney disease: the complete structure of the PKD1 gene and its protein. *Cell* **81,** 289–298 (1995).
19. Ibraghimov-Beskrovnaya, O. *et al*. Strong homophilic interactions of the Ig-like domains of polycystin-1, the protein product of an autosomal dominant polycystic kidney disease gene, PKD1. *Hum. Mol. Genet.* **9,** 1641–1649 (2000).
20. Cai, Y. *et al*. Altered trafficking and stability of polycystins underlie polycystic kidney disease. *J. Clin. Invest.* **124,** 5129–5144 (2014).
21. Gainullin, V. G., Hopp, K., Ward, C. J., Hommerding, C. J. & Harris, P. C. Polycystin-1 maturation requires polycystin-2 in a dose-dependent manner. *J. Clin. Invest.* **125,** 607–620 (2015).
22. Ong, A. C. *et al*. Polycystin-1 expression in PKD1, early-onset PKD1, and TSC2/PKD1 cystic tissue. *Kidney Int.* **56,** 1324–1333 (1999).
23. Qian, F., Watnick, T. J., Onuchic, L. F. & Germino, G. G. The molecular basis of focal cyst formation in human autosomal dominant polycystic kidney disease type I. *Cell* **87,** 979–987 (1996).
24. Chauvet, V. *et al*. Expression of PKD1 and PKD2 transcripts and proteins in human embryo and during normal kidney development. *Am. J. Pathol.* **160,** 973–983 (2002).
25. Mangos, S. *et al*. The ADPKD genes pkd1a/b and pkd2 regulate extracellular matrix formation. *Dis Model Mech.* **3,** 354–365 (2010).
26. Magenheimer, B. S. *et al*. Early embryonic renal tubules of wild-type and polycystic kidney disease kidneys respond to cAMP stimulation with cystic fibrosis transmembrane conductance regulator/Na^+,K^+,$2Cl^-$ Co-transporter-dependent cystic dilation. *J. Am. Soc. Nephrol.* **17,** 3424–3437 (2006).
27. Reif, G. A. *et al*. Tolvaptan inhibits ERK-dependent cell proliferation, Cl^- secretion, and *in vitro* cyst growth of human ADPKD cells stimulated by vasopressin. *Am. J. Physiol. Renal Physiol.* **301,** F1005–F1013 (2011).
28. Taguchi, A. *et al*. Redefining the *in vivo* origin of metanephric nephron progenitors enables generation of complex kidney structures from pluripotent stem cells. *Cell Stem Cell* **14,** 53–67 (2014).
29. Takasato, M. *et al*. Kidney organoids from human iPS cells contain multiple lineages and model human nephrogenesis. *Nature* **526,** 564–568 (2015).
30. Morizane, R. *et al*. Nephron organoids derived from human pluripotent stem cells model kidney development and injury. *Nat. Biotechnol.* **33,** 1193–1200 (2015).

Acknowledgements

The authors thank S. Shankland, E. Kelly, D. Beier, H. Ruohola-Baker and C. Murry (UW), and J. Bonventre, J. Zhou and T. Steinman (Harvard Medical School) for helpful discussions. We thank D. Hailey (ISCRM Garvey Imaging Core) and E. Parker (UW Vision Core Lab) for microscopy support. The Laboratory of Developmental Biology was supported by NIH Award Number R24HD000836 (NICHD). Studies were supported by an NIH Career Development Award K01DK102826 (NIDDK), PKD Foundation Research Award, National Kidney Foundation Young Investigator Grant, and American Society of Nephrology Carl W. Gottschalk Research Scholar Award (B.S.F.). The work was

also supported by start-up funds from the University of Washington, NIH K25HL135432 (H.F.), NIH UH3TR000504 and UG3TR002158 (J.H.), and an unrestricted gift from the Northwest Kidney Centers to the Kidney Research Institute.

Author contributions

N.M.C., S.M.C., R.E.G., A.J.C., Y.K.K., K.W., L.M.T., M.A.D. and B.S.F. performed experiments and analysis of hPSCs and kidney organoids. X.S. and Y.P. performed global gene analysis of kidney organoid cysts. L.S.F., M.A.D. and B.S.F. analysed tissues from PKD patients. N.M.C., X.S., S.M.C., H.F., L.S.F., Y.P., J.H. and B.S.F. contributed to experimental design and analysis. B.S.F. and N.M.C. wrote the first draft of the manuscript. All authors revised the manuscript.

Additional information

Supplementary information is available in the online version of the paper. Reprints and permissions information is available online at www.nature.com/reprints. Publisher's note: Springer Nature remains neutral with regard to jurisdictional claims in published maps and institutional affiliations. Correspondence and requests for materials should be addressed to B.S.F.

Competing financial interests

B.S.F. is an inventor on patent applications for kidney differentiation and disease modelling from human pluripotent stem cells (PCT/US14/34031, PCT/US16/50271).

Methods

Kidney organoid differentiation. WA09 (H9) hPSCs with CRISPR-targeted *PKD1*$^{-/-}$ or *PKD2*$^{-/-}$ mutations, or passage- and procedure-matched non-mutant isogenic controls, were maintained feeder-free on 1% Reduced Growth Factor GelTrex (Life Technologies) in mTeSR1 (Stem Cell Technologies) and dissociated with Accutase (Stem Cell Technologies), as previously described[6]. hPSC lines were derived from either the WA09 hESC line (WiCell) or the WTC11 iPSC line (Gladstone Institute). Identity of parental hPSC lines was confirmed to be correct based on matching the known morphology, karyotype, and pluripotency characteristics of these lines. Cell lines tested negative for mycoplasma. 60,000 cells from each cell line were plated per well of a 24-well plate pre-coated with GelTrex in mTeSR1 supplemented with 10 μM Rho-kinase inhibitor Y27632 (StemGent). The media was replaced with 500 μl mTeSR1 + 1.5% GelTrex at 16 h, 500 μl mTeSR1 at 36 h, Advanced RPMI + Glutamax (from Life Technologies) + 12 μM CHIR99021 (Stemgent) at 50 h, and RB (Advanced RPMI + Glutamax + B27 Supplement, from Life Technologies) at 86 h. RB was changed two days later and every three days thereafter. Alternatively (Protocol B, Supplementary Fig. 6b), undifferentiated hPSCs were plated overnight and then treated with 8 μM CHIR99021 in APEL media (Stem Cell Technologies) for 48–72 h, 30 ng ml^{-1} FGF9 or FGF2 (Peprotech) + 1 μg ml^{-1} heparin (Stem Cell Technologies) in APEL for 96 h, and subsequently cultured in APEL, which was replaced every three days. Organoids typically became visible by light microscopy 12–18 days after plating.

Cyst formation. In adherent cultures (untreated), 'cysts' were identified as large, balloon-like, translucent structures that swayed in response to agitation. Flat rings and dilated tubules were not counted as cysts and occasionally appeared even in non-PKD controls. Forskolin and 8-Br-cAMP (Sigma) were added to adherent cultures on the twenty-first day of differentiation, resulting in rapid formation of cysts that typically did not sway in response to agitation. Wells were imaged using a Nikon TiE inverted wide-field microscope and cysts were quantified using ImageJ cell counter. To generate large cysts in suspension, adherent organoids were microdissected with a 23-gauge syringe needle from 24-well plates on an inverted phase-contrast microscope, and carefully transferred using a transfer pipette into a low-adhesion 6-well plate (Corning) containing 2 ml RB. The organoids were isolated on the twenty-first day of differentiation, before cysts formed. RB media was changed by gravity every three days, and cystogenesis was assessed at two weeks after replating.

Generation of KTEC lines from organoid. To prepare monolayers of kidney cells for analysis, freshly isolated organoids were immediately plated onto tissue culture dishes pre-coated with 1% GelTrex (Thermo Scientific) and cultured for one week in RB, and the resulting epithelial outgrowths were processed for immunoblot and immunofluorescence. Alternatively, to isolate KTECs using flow cytometry, entire organoid cultures were incubated with fluorescein-conjugated LTL (FL-1321, Vector Labs) diluted 1:500 into RB for four hours, dissociated with Accutase, pelleted, resuspended in flow sorting buffer: 1% FBS, 10 mM HEPES buffer in phosphate buffered saline (PBS) (Thermo Scientific). LTL^{+} cells were isolated on a FACSAria Cell Sorter (BD Biosciences) and replated onto GelTrex-coated tissue plates in RB.

Organoid embedding in collagen droplet. To embed organoids in collagen droplets, a sheet of Parafilm was soaked in 70% ethanol, air dried, and pressed against the holes of a box of gel-loading pipette tips (1–200 μl, Fisher Scientific 02-707-138) to create a dimpled mould[31]. One organoid was placed in each dimple and 30 μl of 7 mg ml^{-1} collagen I (Corning) was added. The droplets were incubated 25 min at 37 °C and carefully resuspended in 3 ml of RB media in an untreated 6-well plate. The media was changed weekly and the droplets were imaged after two weeks of incubation using a Nikon Ti Inverted Wide-field microscope and a Nikon 1 J1 Camera. Droplet diameters were measured using NIS Elements imaging software (Nikon) and normalized to the diameter of empty droplets from the same set, for a total of three sets. Droplets that failed to undergo compaction (∼20% in control and ∼50% in PKD samples) were excluded. Droplets were fixed with 4% paraformaldehyde (PFA) for 20 min at room temperature, incubated 16 h in 30% sucrose (Sigma) in water, mounted in Tissue-Tek (Sakura), flash frozen, and cryosectioned onto SuperfrostPlus slides (Fisher). Sections were stained in Picro-sirius red solution (Sky-Tek laboratories) for one hour, rinsed in two changes of 0.5% acetic acid solution, and dehydrated in two changes of absolute ethanol before mounting. Immunofluorescence was performed as described below.

siRNA and immunoblotting. 16 h after plating, hPSCs were transfected with Dharmacon Smartpool siRNAs (Fisher Scientific) directed against *PKD2* or scrambled control in mTeSR1 without antibiotics. Media was changed 24 h later. 72 h after siRNA treatment, cells were lysed in RIPA buffer (Thermo Scientific) containing 1× Complete mini EDTA-free protease inhibitor, PhosSTOP, and benzonase nuclease (all Sigma). Protein lysates were quantified using a BCA protein assay kit (Thermo Fisher). To prepare the samples, 50 μg of protein were mixed with Pierce Lane Marker Reducing Sample (Thermo Fisher) and incubated at 40 °C for 5 min. Samples were separated in a 4–20% protein gel (Bio-Rad) and transferred into a PVDF membrane using standard protocols and 0.01% SDS in the transfer buffer (0.25M Tris Base, 1.92M Glycine, 0.1% SDS). Gels included pre-stained molecular weight markers (Precision Plus Protein Kaleidoscope Standards, Bio-Rad), which were annotated manually by overlay of the film onto the nitrocellulose membrane. The antibodies used for the immunoblots were anti-PC1 (sc-130554, Santa Cruz), anti-PC2 (sc-10376, Santa Cruz) and anti-β-actin (4970S, Cell signaling). The intensity ratio of the experimental band to the loading control was normalized to 1 in the negative control (unmodified or untreated hPSCs). The remaining bands were normalized to the control and averaged for at least three independent experiments. Examples of unprocessed immunoblots with the original standards hand-marked are provided in Supplementary Fig. 7.

Global gene expression and bioinformatics analysis. For systems biology analysis of cysts, cystic epithelium or tubule remnants were manually separated from *PKD1*$^{-/-}$ organoids (71–87 days of culture from three experiments) using a 22-gauge needle under a dissecting microscope and flash frozen separately in liquid nitrogen. Total RNA containing small RNA was extracted from seven paired samples (cysts and tubule remnants from the same organoid) using RNeasy Micro Kit (Qiagen) with an on-column DNA digestion step to minimize genomic DNA contamination. The sample integrity of the RNA was assessed using the RNA 6000 Nano Assay on 2100 Bioanalyzer (Agilent Technologies) to ensure that RNA integrity number (RIN) was greater than 7. Microarray experiments were performed at The Centre for Applied Genomics (TCAG) at the Hospital for Sick Children. Following the manufacturer's protocol, 10 ng of total RNA was labelled using the GeneChip WT Pico Reagent Kit (Affymetrix). Fragmented and biotin-labelled ss-cDNAs were then hybridized to GeneChip Human Gene 2.0 ST Arrays (Affymetrix) for 16 h at 4 °C. Hybridized arrays were stained and washed in the Affymetrix Fluidics Station 450. Thereafter, the arrays were scanned on an Affymetrix GeneChip Scanner 3000 and the image (.DAT) files were preprocessed using the Affymetrix GeneChip Command Console (AGCC) software v.4.3 to generate cell intensity (.CEL) files. After image processing, the array data were uploaded to the Affymetrix Expression Console software v1.4.1 for further processing and quality control. All quality assessment metrics, including spike-in controls during target preparation and hybridization were found within the boundaries. The probe set signal intensities were then extracted and normalized using the robust multi-array average (RMA) algorithm embedded in the Expression Console software, which consists of convolution background correction, quantile normalization, and median polish summarization. Downstream paired sample *t*-test was carried out via Partek Genomics Suite 6.6 (Partek) to determine differentially expressed genes between cysts and tubules. Gene set enrichment analysis (GSEA, http://software.broadinstitute.org/gsea/index.jsp) was used as the primary tool to identify potential gene pathways or gene sets that may modulate cystic kidney organoid growth[32]. Before running GSEA, Affymetrix probe sets were collapsed to one gene level, paired sample *t*-test statistics scores were used to create a ranked list of genes of the entire data set (in total, 29406 unique genes with gene symbols). GSEA was performed using the Hallmark gene sets from Molecular Signatures Database (MSigDB, http://software.broadinstitute.org/gsea/msigdb/collections.jsp#H)[33]. The description of each gene set can be found on the MSigDB website. We defined overrepresented gene sets with a false discovery rate (FDR) ≤ 0.25. For RNA-Seq analysis of hPSCs, RNA was prepared from isogenic sets of cell lines using the RNEasy Mini Kit (Qiagen), checked for high integrity on an Agilent Bioanalyzer, prepared using the TruSeq stranded mRNA library kit (Illumina), and sequenced on an Illumina NextSeq500 75 × 75 paired-end high-output run. Samples were aligned to an hg19 reference sequence.

Immunofluorescence. To fix organoids, an equal volume of 8% paraformaldehyde (Electron Microscopy Sciences) in PBS was added to the culture media (4% final concentration) for 15 min at room temperature. After fixing, samples were washed in PBS, blocked in 5% donkey serum (Millipore)/0.3% Triton X-100/PBS, and incubated overnight in 3% bovine serum albumin/PBS with primary antibodies. The next day, samples were washed in PBS and incubated overnight with Alexa-Fluor secondary antibodies and DAPI (Thermo Scientific), followed by PBS washes. For frozen tissue sections, fresh tissues were incubated in 4% paraformaldehyde for one hour at 4 °C, incubated 16 h in 30% sucrose (Sigma) in water, mounted in Tissue-Tek (Sakura), flash frozen, and cryosectioned onto SuperfrostPlus slides (Fisher) before blocking. Paraffin sections were prepared by fixing overnight in methacarn (60% absolute methanol, 30% chloroform, 10% glacial acetic acid, Sigma) or in 4% PFA, followed by paraffin embedding, sectioning, deparaffinization in 100% xylene (3 washes, 5 min each), dehydration in graded 70%–100% ethanol (5 min each), and heating in citrate buffer pH 6.0 (Sigma) in a pressure cooker (Instant Pot IPDUO60) for three minutes prior to immunostaining. Kidney organoid cysts were embedded in 2% agarose prior to paraffin embedding. Histology stains (Haematoxylin and eosin, or Masson's trichrome) were applied to paraffin sections by UW Pathology. Primary antibodies

included acetylated alpha-tubulin (051M4770; Sigma), ZO-1 (339100; Invitrogen), LTL (FL-1321, Vector Labs), PC2 (sc-25749, Santa Cruz), NPHS1 (R&D AF4269, 1:500), KIM-1 (MAB1750, R&D), PODXL (R&D AF1658, 1:500), ECAD (Abcam ab11512), SMA (Sigma A2547, 1:500), LAMA1 (Sigma L9393a, 1:500), and pH3 (sc-8656, Santa Cruz). Fluorescence images were captured using a Nikon epifluorescence 90-I (upright), Nikon Ti Inverted Wide-field microscope, or Nikon A1R and C1 confocal microscopes. pH3+ cells were scored manually in cysts or tubular organoids of similar sizes.

Electron microscopy. Droplets were gently transferred with a cut-off transfer pipette into EM fix: 0.15 M sodium cacodylate trihydrate (Sigma) dissolved in water (pH 7.3) containing 4% formaldehyde and 2% glutaraldehyde (Electron Microscopy Sciences), and stored overnight. Samples were post-fixed with osmium tetroxide solution (Sigma), dehydrated in serial ethanol dilutions (Sigma), and embedded in epoxy resin. Ultrathin sections (80 nm) were mounted on 200 mesh copper grids and stained with uranyl acetate and lead citrate (Electron Microscopy Sciences). Imaging was performed with a JEOL JEM-1010 TEM and a FEI Tecnai G2 Spirit TEM.

PKD patients. All human samples were obtained with informed consent and in compliance with all ethical regulations under the auspices of protocols approved by the UW Institutional Review Board. These included an ADPKD kidney donated by a 46-yr-old female (generous gift of Virginia Mason Hospital), an anonymized biopsy of a 15-week control kidney (UWLaboratory of Developmental Biology), and anonymized biopsies of kidneys with clinically diagnosed Meckel syndrome (20 weeks), ARPKD (29 weeks, 6 months, or 6 years.), and orofaciodigital syndrome (18 yr.) from Seattle Children's Hospital Histopathology. Patients with kidney disease were enrolled in our study for the purposes of collecting cells and tissues as positive controls. These samples were collected from patients of all ages without any discrimination with respect to gender, age, race, family history, or other co-variates. PKD samples were chosen from this collection at random and based on availability to represent a range of disease severities, ages, and genotypes.

Statistical analysis. Experiments were performed using a cohort of PKD hPSCs, generated as described previously[6], including three *PKD1*$^{-/-}$ and two *PKD2*$^{-/-}$ hPSC lines, and a total of six isogenic control lines that were subjected to CRISPR mutagenesis but were found to be unmodified at the targeted locus. Quantification was performed on experiments performed side by side on at least three different occasions. Error bars are mean ± standard error (s.e.m.). Statistical analyses were performed using GraphPad Prism Software. To test significance, p values were calculated using two-tailed, unpaired t-test with Welch's correction (unequal variances). Statistical significance was defined as $p < 0.05$. Exact p values, t values and degrees of freedom are provided in the figure legends.

Data availability. Microarray data are MIAME compliant and publicly available in Gene Expression Omnibus (GEO, http://www.ncbi.nlm.nih.gov/geo) (ID: GSE101308). All remaining datasets are available from the corresponding author upon reasonable request.

References

31. Lancaster, M. A. *et al*. Cerebral organoids model human brain development and microcephaly. *Nature* **501,** 373–379 (2013).
32. Subramanian, A. *et al*. Gene set enrichment analysis: a knowledge-based approach for interpreting genome-wide expression profiles. *Proc. Natl Acad. Sci. USA* **102,** 15545–15550 (2005).
33. Liberzon, A. *et al*. The Molecular Signatures Database (MSigDB) hallmark gene set collection. *Cell Syst.* **1,** 417–425 (2015).